33RD CONGRESS
OF THE INTERNATIONAL COUNCIL
OF THE AERONAUTICAL SCIENCES
STOCKHOLM, SWEDEN, 4–9 SEPTEMBER, 2022

ICAS
2022
SWEDEN

ANALYSIS OF THE STABILITY OF MULTIPLE HELICAL VORTICES USING COMPLEX-STEP LINEARIZATION

V. G. Kleine[1,2], A. Hanifi[1] & D. S. Henningson[1]

[1]FLOW, Dept. of Engineering Mechanics, KTH Royal Institute of Technology, Sweden
[2]Division of Aeronautical and Aerospace Engineering, Instituto Tecnológico de Aeronáutica, Brazil

Abstract

The system of vortices created by the hub and tip vortices of rotors and propellers is composed of two subsystems of helical vortices that have different radii and pitches. A similar system of external and internal vortices is created by some blade devices proposed to destabilize the tip vortices of helicopters. The steady solution of these systems of vortices was recently described. However, their stability was not studied. The stability of a system of multiple helical vortices was studied in this work using a complex-step technique to linearize the Biot-Savart law and the vorticity transport equations. It was noted that the hub and tip vortices do not interact and their linear stability can be treated separately, if the velocity field induced by one system is considered in the stability of the other. For a ratio of radius of 0.8, strong interaction between the vortices was observed, with an out-of-phase mechanism appearing as one of the main phenomena.

Keywords: rotor, tip device, stability, vortex, fluid mechanics

1. Introduction

The blades of rotors generate a system of helical vortices. The stability of helical vortices has been related to the dangerous vortex ring state in the wake of descending helicopters [1] and vortex-structure interaction in certain flight regimes of rotorcrafts [2]. Additionally, in wind farms, the instabilities of tip vortices affect the near wake and, consequently, can affect the power production and fatigue of a downstream wind turbine [3, 2]. Hence, the study of hydrodynamic stability of tip vortices has gained the interest of the rotor aerodynamics community. Analytical investigation of the stability of helical vortices has been performed by [4] and [5]. Several recent numerical and experimental studies showed agreement with the theory [6, 7, 1, 8]. These stability studies have focused on uniform helices (all helical vortices with the same pitch, radius and circulation).

The creation of multiple non-uniform helical vortices has been suggested as a way to destabilize the tip vortices. Some devices, such as flaps and blade tip devices, have been proposed as mechanisms to modify the circulation to generate two vortices near the blade tip of helicopters [9] and wind turbines [10, 11]. These devices have the potential to reduce noise and other negative effects of blade-vortex interaction in helicopters [9, 12, 2]. Schröder *et al.* [12, 2] cited multiple stability mechanisms that could be relevant for the dynamics of the vortices created by these devices, including long-wave instability of the vortices.

Also, even for the most basic rotor, the system of vortices created by the hub and tip vortices of rotating blades is composed of two systems of vortices that have different radii and pitches, hence, cannot be fully studied using the previously mentioned analytical methods [4, 5].

Recently, a method for obtaining the equilibrium solution of the interacting helical pairs with different pitches and radii was published by [13], but the stability of the system was not addressed. Only a handful of cases were previously investigated by [14] using a vortex method, where helical vortices with different radii but the same pitch were studied. A study of the stability of a system of internal and external vortices with different pitches and radii could not be found in the literature.

The current work aims to study the stability of the system consisting of multiple helical vortices in incompressible flow. A method based on the linearization of the Biot-Savart law and the vorticity transport equation using complex-step is proposed and discussed in the present work. This method reduces the errors and improves the accuracy of the linearization, when compared to the same approach using real disturbances.

During the preparation of this paper, the authors became aware of the work of [15], that also uses a discretized representation of vortices to study the growth of long-wave instabilities composed of Fourier modes. Their method is based on the linearization of the equations through evaluation of the derivatives numerically, while our method uses a time integration, as described in section 2.. Both methods can be applied to any periodical configuration of vortices. We are interested in configurations of vortices where an external and an internal system can be clearly defined. In this configuration, the radial position of the helices change (see [13]) but their relative position is unmodified: it is always possible to identify if a vortex is an internal or external vortex. On the other hand, Castillo-Castellanos & Le Dizès [15] studied closely spaced co-rotating helical vortices described in [16], where the interaction of the two subsystems of vortices change their relative radial position, similar to leapfrogging configurations.

As far as the authors are aware, the technique of combining the complex-step method with a time marching operator to study the linear stability of flows is first applied here.

The method proposed here aims to study the long-wave instabilities, focusing primarily on double triple helical vortex systems composed of three external vortices and three internal vortices. The effect of the hub vortices on the stability of the tip vortices (and vice-versa) is investigated. Also, within the limits of the long-wave theory [1], we study the stability of a configuration where the radial position of the internal vortices is 80% of the external vortices, which model two systems of helical vortices generated near the tip of each blade, to understand if the long-wave mechanism can guide the design of flap or wingtip devices that destabilizes the flow.

2. Methods

2.1 Governing equations

From the Biot-Savart law and the vorticity transport theorem, the velocity $\mathbf{U}$ induced by a system of N_v vortices at point $\mathbf{x}$ is given by:

$$\frac{d\mathbf{x}}{dt} = \mathbf{U}(\mathbf{x}) = -\sum_{m=1}^{N_v} \frac{\Gamma_m}{4\pi} \int \frac{(\mathbf{x} - \mathbf{x_m}) \times d\mathbf{L_m}}{|\mathbf{x} - \mathbf{x_m}|^3} \tag{1}$$

where Γ_m is the circulation of vortex of index m and $d\mathbf{L_m}$ is the elemental length vector of the segment of vortex located at $\mathbf{x_m}$.

Equation (1) has a singularity (at $\mathbf{x} = \mathbf{x_m}$), which is usually treated by a desingularization strategy. We adopt the Rosenhead-Moore approximation [17, 18] of the Biot-Savart law when evaluating the integral for the vortex that contains the control point $\mathbf{x}$. This is the same method used by [5]. In this method, the denominator is modified by a factor ε_0, which is $\varepsilon_0 = e^{-3/4}a$, where a is the radius of the vortex core [19, 1] for a uniform core without axial flow.

Using equation (1), it is possible to discretize the vortex filaments in small segments and follow their displacement, as described in [20, 13]. All the cases analyzed here are periodic in the z-direction (axial direction of the helices). Each period is discretized with n_c control points, which are the position of the fluid particles which are followed in order to define the steady-state and study the evolution of perturbations. To increase the accuracy of the computation of the velocity induced by the Biot-Savart law for the curved vortices present in the configuration, the vortices between the control points are further refined, with n_s vortex segments. The total number of vortex segments per period is then $n_c n_s$. The position of the segments is interpolated from the position of the n_c control points using a Fourier interpolation.

Equation (1) is applied to fluid particles. However, we want to follow the spatial displacement of the vortex structure, not the fluid particles. For a deeper discussion of these concepts, see [21]. To distinct these concepts, we denote the position of the vortical structure as $\mathbf{r}$.

2.2 Steady state

As described by [13], there is a rotating and translating frame of reference in which the vortex system can be considered steady. In this steady state, the velocities are constant and the helical structures are static, however, the fluid particles move along the helices with the tangential velocity. The Biot-Savart law (with a desingularization technique) and the vorticity transport theorem are used to find the velocities of the fluid particles. Knowing the velocity of the fluid particles, the position of the vortical structure, $\mathbf{r}$, as a function of the streamwise coordinate z, can be determined, as done in [13]. The vortex filaments are discretized in small segments and the induced velocity at each control point is calculated. We end up with a system of equations that can be written as

$$\frac{d\mathbf{r}}{dt} = \mathcal{N}(\mathbf{r}) \tag{2}$$

where $\mathcal{N}$ is a non-linear operator. The steady solution $\mathbf{r}_0$, for which $\mathcal{N}(\mathbf{r}_0) = 0$, can be found numerically using a relaxation method (iterative method) [13].

2.3 Complex-step linearization

To study the stability of the system, a complex-step linearization process is proposed, in order to reduce errors. Analogously to complex-step differentiation [22], a complex perturbation $i\delta\mathbf{r}$ ($\delta\mathbf{r}$ real) is imposed to the known steady solution

$$\frac{d(\mathbf{r}_0 + i\delta\mathbf{r})}{dt} = i\frac{d\delta\mathbf{r}}{dt} = \mathcal{N}(\mathbf{r}_0 + i\delta\mathbf{r}). \tag{3}$$

The application of the Taylor series expansion gives

$$\mathcal{N}(\mathbf{r}_0 + i\delta\mathbf{r}) = \mathcal{N}(\mathbf{r}_0) + iJ_{\mathcal{N}}(\mathbf{r}_0)\delta\mathbf{r} + \mathcal{O}(i^2\delta\mathbf{r}^2), \tag{4}$$

where $J_{\mathcal{N}}$ is the Jacobian of the non-linear operator and $\mathcal{O}$ represents the order of the remaining terms. Ideally, $\mathcal{N}(\mathbf{r}_0) = 0$. However, the numerical relaxation process may lead to errors that might affect the stability analysis. Taking the imaginary part of the previous equations

$$\frac{d\delta\mathbf{r}}{dt} = imag(\mathcal{N}(\mathbf{r}_0 + i\delta\mathbf{r})) = J_{\mathcal{N}}(\mathbf{r}_0)\delta\mathbf{r} + \mathcal{O}(\delta\mathbf{r}^3) \tag{5}$$

not only the errors in the steady solution are removed but the order of the approximation is increased to third order. Neglecting the third-order terms and integrating in time we arrive at

$$\delta\mathbf{r}(t) = imag\left(\int_0^t \mathcal{N}(\mathbf{r}_0 + i\delta\mathbf{r})dt\right) \approx e^{J_{\mathcal{N}}t}\delta\mathbf{r}(0). \tag{6}$$

The term $\int_0^t \mathcal{N}(\mathbf{r}_0 + i\delta\mathbf{r})dt$ is calculated using a time-stepping free vortex method (section 2.4). Hence the full, non-linear, time evolution operator can be used as a black-box with a small complex disturbance $i\delta\mathbf{r}(0)$ to find the linear time evolution operator $e^{J_{\mathcal{N}}t}$. For large problems, one possibility to calculate the eigenvalues of the linear operator is to employ the iterative time-stepping technique with the Arnoldi iteration [23]. However, for small problems such as the present, the linear operator $e^{J_{\mathcal{N}}t}$ can be reconstructed by imposing the standard basis (or any basis) as the disturbance $\delta\mathbf{r}(0)$.

The eigenvalues λ_j of $J_{\mathcal{N}}$ are obtained from the eigenvalues of μ_j of $e^{J_{\mathcal{N}}t}$, $\lambda_j = \log(\mu_j)/t$, and the eigenvectors of $J_{\mathcal{N}}$ and $e^{J_{\mathcal{N}}t}$ are the same [23]. Validation was performed by applying this method to simple helical vortices and the results agree well with [5].

2.4 Time-stepping free-vortex method

A forth-order Runge-Kutta scheme is used to integrate equation (1) in time. As a free-vortex method (see [20]), this is initially a Lagrangian approach, following fluid particles. However, we want to follow the spatial displacement of the vortex structure, not the fluid particles, as mentioned in previous sections. Because of this, for every stage of the Runge-Kutta integration, first the position of the fluid particles is obtained and then the position of the vortex structure is found by fitting Fourier series. The
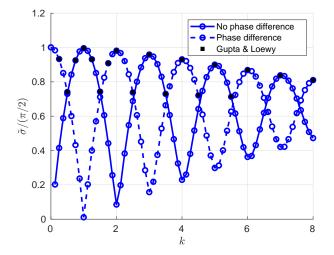
Figure 1 – Comparison of the growth rates calculated with the current method (in blue) with the results of [24, 5] (black symbols) for a two-bladed rotor. Only modes with positive growth rate are shown.

position of the vortex structure is hence defined as a function of the original grid uniformly distributed in the streamwise coordinate z.

Since the streamwise coordinate is used also as a parametrization parameter, some ambiguity could arise if real perturbations were used. Due to characteristics of helical vortices, some displacements in the streamwise directions are indistinguishable from displacements in the azimuthal direction. The use of complex disturbances avoids this ambiguity, as the real part of z is used as the parametrization parameter and we are interested only in the imaginary part of the displacements.

3. Results

3.1 Validation

The results of the method were compared to the results of [24, 5] for a two-bladed rotor. As can be seen in figure 1, the growth rates are practically identical for the eigenvalues where data from [24] is available. To aid the interpretation of the figure, the modes for which the disturbances do not have phase difference and the modes for which the disturbances have a phase difference of π are grouped (see [8] for further discussion about these modes).

These results were obtained with a discretization of $n_c = 32$ control points per turn of the helix. Between each control point, vortices are discretized with $n_s = 16$ segments, to increase the accuracy of the computation of the velocity induced by the Biot-Savart law. Disturbances in the order of $1 \cdot 10^{-6}$ were imposed, using the standard basis (vectors composed by all elements equal to zero, except one element equal to 1). The integration in time is performed in a single step, for a time-step of $t = 1 \cdot 10^{-5}$. These parameters are used for the other cases of this work.

3.2 Tip vortices and hub vortices

The parameters of the vortical systems studied are listed in table 1. We chose to maintain the pitch (h) and vortex core size (a) constant and change the radius of the internal vortices (subscript $_{ext}$ refers to the external vortex subsystem and subscript $_{int}$ refers to the internal). The cases with the circulation with opposite signs can represent tip and hub vortices created by a single set of blades. The case with circulation with the same sign can represent a vortex system generated by flaps or other devices used to create multiple vortices along the blades.

The first case considered is an example of the most common system of double triple helices: a hub and tip vortex configuration. The case most representative of tip and hub vortices is Case 1, which can be seen in figure 2. Case 2 can also be considered tip and hub vortices created by a simple set of 3 blades, however, the radial position of the internal helices is higher than usual for a propeller or wind turbine. Case 2 is relevant, however, to study the interaction of multiple unstable systems

4

of vortices, because in Case 1 the hub vortices are stable to the imposed disturbances. Case 3 is discussed in section 3.3

Case	R_{ext}	h_{ext}	Γ_{ext}	a_{ext}	R_{int}	h_{int}	Γ_{int}	a_{int}	R^*	α
Case 1	1	2	-1	0.03	0.2	1.75	1	0.03	0.2	7/8
Case 2	1	2	-1	0.03	0.4	1.75	1	0.03	0.4	7/8
Case 3	1	2	-1	0.03	0.8	1.75	-1	0.03	0.8	7/8

Table 1 – Parameters of the system of vortices. Radius (R), pitch (h), circulation (Γ), vortex core size (a), ratio of radius ($R^* = R_{int}/R_{ext}$) and ratio of pitch ($\alpha = h_{int}/h_{ext}$).

Figure 2 – Steady state system of tip and hub vortices. The initial properties of the system are shown in table 1, Case 1. The actual radial and azimuthal positions, plotted in this figure, are found after the helix deformation obtained using the method of [13]. As explained by [13], for this system, the deformations are very small (imperceptible to the naked eye).

In order to understand the mutual influence of the two subsystems of vortices, the growth rate was obtained using three models:

1. Full vortex system, considering all possible mutual inductance mechanisms;

2. Tip (hub) vortices inside the velocity field induced by the undisturbed hub (tip) vortices (matrix $e^{J_\mathcal{N} t}$ is cropped, discarding disturbances of hub (tip) vortices);

3. Isolated vortices. Stability of tip (hub) vortices calculated without considering hub (tip) vortices. The method is applied again for only one triple helix at a time. The results should be equivalent to the model of [5].

In figures 3 and 4 the growth rate of the disturbances is shown as a function of the wavenumber. The growth rate σ (real part of the eigenvalues) is normalized using the properties of the tip vortex $\tilde{\sigma} = 2(h_{ext}/3)^2/|\Gamma_{ext}|\sigma$, in order to compare to the maximum growth rate of a 2-d row of vortices ($\pi/2$) [25, 19], identified in several previous works [7, 1, 8, 26, 27] as relevant for the stability of helical vortices of low pitch. Using the normalization with the parameters of the tip vortices, the theoretical growth rate of $\pi/2$ for the hub vortices is shown in figure 3(b) and 4(b) by the dashed line, $\tilde{\sigma}/(\pi/2) = 1/(\alpha)^2 \approx 1.3$. The growth rate of a 2-d row of vortices models well the maximum growth rate of the tip vortices, however, the growth rate of hub vortices may differ from this model due to the high values of pitch to radius ratio. In particular, for Case 1, the subsystem of hub vortices is stable, both in isolation and in the velocity field of the tip vortices, as can be seen by the absence of dots and crosses in figure 3(b). On the other hand, for Case 2, the maximum growth rate of the hub vortices is greater than the tip vortices, as expected for the model of 2-d row of vortices due to its lower value of pitch. More elaborate models for the analogy with the row of 2-d vortices, that gives a more accurate growth rate for helices of low pitch, are described in [1, 8]. These models explain the reason for the higher growth rate in figure 4(b) when compared to the simpler model of $\tilde{\sigma}/(\pi/2) \approx 1.3$. However, in order to keep the same reference irrespective of the radius of the internal vortex, we include only the simpler model as the dashed black line in the figures.

The model of the full vortex system allows disturbances of the hub to influence the disturbances of the tip (and vice-versa), while this is not possible in the other models. Hence, the same eigenvalue
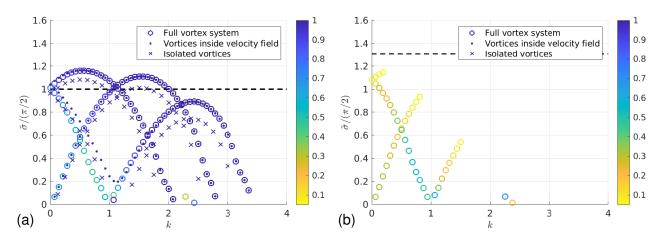
Figure 3 – Normalized growth rate calculated for the tip vortices (left) and hub vortices (right) in function of the wavenumber (k), for Case 1. Dashed black line indicates growth rate of 2-d row of vortices [25, 19]. Colors of circles (full vortex system model) indicate the percentage of the eigenvector that belongs to the tip or hub vortices (described in the main text).
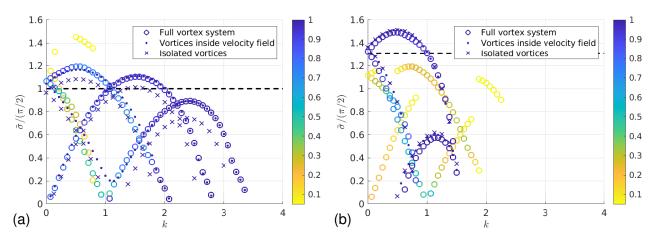

Figure 4 – Normalized growth rate calculated for the tip vortices (left) and hub vortices (right) in function of the wavenumber (k), for Case 2.

(whose real part is indicated by the growth rate σ) can appear simultaneously in the plot of the tip and hub in figures 3 and 4. To indicate the relative contribution of each subsystem of vortices, colors are used. The colors of the circles indicate the percentage of the eigenvector that belongs to the tip or hub vortices. The eigenvector is split into two parts, a hub and a tip component, then the square of the norm of each part is used as the metric that defines the percentage. Consequently, a light yellow circle in the hub plot means that this mode has most of its energy in the tip and there is a corresponding blue circle in the tip plot (and vice-versa), with a different wavenumber but the same normalized growth rate. All the modes of the models of vortices inside velocity field (dots) and isolated vortices (crosses) are represented in dark blue, since these models do not allow interaction between disturbances at the tip and hub vortices.

In figure 3(b), for example, we see, by the yellow, green and light blue circles, that there are many modes predicted by the full vortex system model that do not have a correspondence in the isolated vortex model or the velocity field model. Since the hub vortices are stable for this case, all these are modes driven by the instabilities of the tip vortices. It can be noted that the main modes (higher growth) for this system involve almost exclusively the tip vortices (figure 3(a)) and, therefore do not show great interaction between hub and tip vortices.

The same qualitative behaviour can be observed in figure 4(b). Even though the hub vortices are unstable for this case, a few of the modes of the tip vortices induce other instabilities on the hub

vortices. However, the most relevant modes of the hub are not modified by the presence of the tip vortices. Hence, the modes with higher growth rates do not show interaction between internal and external helices.

As can be seen in figures 3(a) and 4(a), the tip vortices are more unstable due to the presence of hub vortices, when compared to the model with isolated tip vortices. However, this is due to the velocity field of the undisturbed hub vortices. The disturbances of the hub vortices, in general, do not interact with the most relevant modes of the tip vortices. The results are consistent with previous result of [28], that showed that tip vortices are less stable if a concentrated hub vortex (Joukowski's model) is considered, due to the induced velocity field. However, their model was not able to account for the mutual interaction, which we show to be negligible for this case.

3.3 Multiple vortices near the tip

Case 3 is a configuration in which the vortices have the same sign and are close to each other, modeling multiple vortices generated near the tip by the same blade, for example, by a flap. Another example is two in-line rotors under very low disturbance flow, as seen in [29]. Such configurations would probably have hub vortices. However, in this work we do not consider the hub vortices for this case.

If the generation of the vortices is too close to each other, there would be a strong interaction and the configuration formed by closely spaced co-rotating vortices described in [16] would be created. The stability of these co-rotating vortices is studied in [15]. The configuration studied here, with a ratio of radius $R^* = 0.8$, has a clear distinction between an internal system of vortices and an external system of vortices.

Figure 5 shows that there is great interaction between the vortices for this case. The model with the full vortex system presents results considerably different from the model of vortices inside velocity field and the model of isolated vortices.
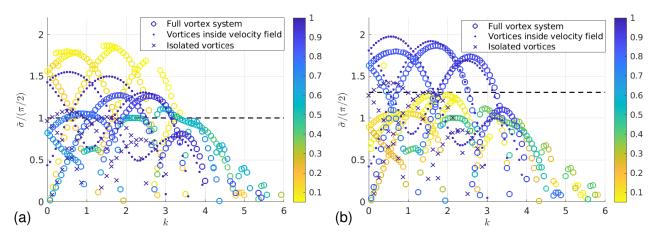

Figure 5 – Normalized growth rate calculated for the external vortices (left) and internal vortices (right) in function of the wavenumber (k), for Case 3.

The interaction of vortices changes the stability in a quantitative and qualitative way. The effect of the velocity field is more quantitative, but it preserves some of the qualitative aspects of the stability of isolated vortices. Comparing the model with vortices inside the velocity field and the model of isolated vortices, the growth changes but the wavenumber corresponding to the peaks are approximately the same, following the rule $k = (j + 1/2)$ where j is any integer (for an odd number of blades). Also, the larger peaks occur for lower wavenumbers (as described in [8]). The interaction of vortices of different subsystems modifies this trend. Comparing the full vortex system model with the model of vortices inside the velocity field, the interaction between vortices reduces the growth for low wavenumbers.

An important difference occurs on the wavenumbers with maximum growth, which deviate from the values $k = (j + 1/2)$. For example, the maximum growth of a mode dominated by the external vortices (blue circles in figure 5) shifts to $k \approx 1.8$. The eigenvector corresponding to this mode is shown in figure 6. Looking only at the tip vortices (in blue, green and cyan), a sub-optimal out-of-phase vortex

pairing can be noticed. Even though this mode is dominated by the external vortices, components in the internal vortices (in red, yellow and brown) can be observed. These components seem to be out of phase with the disturbances in the external vortices, with a very similar wavenumber. This could be an explanation for the shift in the wavenumber of maximum growth: the instabilities appear to favor wavenumbers that could match a disturbance in the internal vortices.
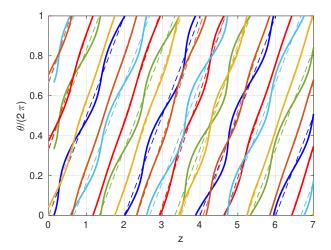

Figure 6 – Unrolled representation of the eigenvector of the mode with the highest growth rate among modes dominated by external vortices ($k_{ext} \approx 1.8$). The figure is not periodic, only a representative part of the eigenvector is shown. Dashed lines are the undisturbed vortices. Blue/green/cyan corresponds to external vortices. Red/yellow/brown corresponds to internal vortices.

Also, new branches that are almost equally balanced between the external and internal vortices appear (in green in figure 5). One of these modes, with $k_{ext} \approx 1.8$ and $\tilde{\sigma}/(\pi/2) \approx 1$ is be presented in figure 7. For this mode, the out-of-phase mechanism between internal/external vortices is even more pronounced. A similar phenomena was observed in [29], for wavenumber $k_{ext} = 3$, which correspond to a mode that is originally stable for isolated vortices (for disturbances without phase difference between blades, as in [29]).
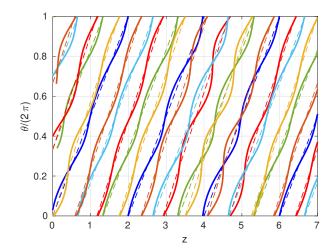

Figure 7 – Unrolled representation of the eigenvector of one of the modes with external vortices and internal components (mode with $k_{ext} \approx 2.0$ and $\tilde{\sigma}/(\pi/2) \approx 1$ in figure 5(a)). The figure is not periodic, only a representative part of the eigenvector is shown. Dashed lines are the undisturbed vortices. Blue/green/cyan corresponds to external vortices. Red/yellow/brown corresponds to internal vortices.

The out-of-phase mechanism has also been observed by [15] in closely spaced co-rotating helical

vortices. There is the possibility that these are manifestations of the same effect. Also, there is the possibility that these mechanisms would give rise to the braided helices mentioned in [16, 15] if the distance between the vortices is reduced. Further studies are needed to understand all the modes of this configuration and their consequence.

4. Conclusions

A new method for studying the stability of vortices, which combines a complex disturbance with a time integration algorithm is proposed and validated. For the configuration of a single system of helical vortices, the method gives results equivalent to results found in the literature that employs an analytical approach [5]. To the best of our knowledge, the use of integration in time in conjunction with a complex-step technique to linearize a dynamical system (instead of the more usual complex-step differentiation, for example) is first proposed in this work.

The long-wave stability of a system of multiple vortices composed of helices of different radii and pitches is studied using this method. The results presented here indicate that if the ratio of radius is low, the main modes of the external vortices and the internal vortices do not interact. This indicates that the hub vortex linear instabilities do not affect the tip vortices (and vice-versa). There is an effect of the presence of the hub vortices, however, this influence is restricted to the velocity field induced by the undisturbed vortices. These results suggest that proposed methods to destabilize the tip vortices by actuation on the hub vortices would probably not be successful if they rely on a linear stability mechanism.

It should be noticed that this conclusion is restricted to the linear mechanism and small perturbations. The growth of the small disturbances on a subsystem of vortices would lead to higher disturbances and non-linear interaction. For example, in [27], large disturbances are observed a few radii downstream of a moving wind turbine both for the tip and hub vortex subsystems. The flow structures created by these large disturbances certainly affect the other subsystem of vortices.

For internal and external vortices close to each other, with a ratio of radius $R^* = 0.8$, the interaction is much stronger. The growth rates of the full vortex system deviate from the growth rate of isolated vortices. For this case, the effect cannot be attributed to the velocity field. The interaction of the vortices could be observed in some of the eigenvectors, where the external vortices appear as out-of-phase to the internal vortices. Studies to further understand these modes and their consequence are ongoing.

The proposed method and presented results may contribute to elucidating the mechanisms of stability of vortices created by rotors, including the interaction between tip and hub vortices, and also between multiple vortices created by devices proposed to be installed on helicopter or wind turbine blades. The understanding of different mechanisms of vortex interaction and stability could guide the design of flaps or devices for rotors that could reduce noise or problems related to vortex-structure interaction.

Contact Author Email Address

Vitor G. Kleine: vitok@mech.kth.se

References

[1] Quaranta H U, Bolnot H and Leweke T. Long-wave instability of a helical vortex. *Journal of Fluid Mechanics*, Vol. 780, pp 687–716, 2015.

[2] Schröder D, Aguilar-Cabello J, Leweke T, Hörnschemeyer R and Stumpf E. Experimental investigation of a rotor blade tip vortex pair. *CEAS Aeronautical Journal*, Vol. 13, No. 1, pp 97–112, 2022.

[3] Sørensen J N, Mikkelsen R F, Henningson D S, Ivanell S, Sarmast S and Andersen S J. Simulation of wind turbine wakes using the actuator line technique. *Philosophical Transactions of the Royal Society A: Mathematical, Physical and Engineering Sciences*, Vol. 373, No. 2035, p. 20140071, 2015.

[4] Widnall S E. The stability of a helical vortex filament. *J. Fluid Mech.*, Vol. 54, No. 4, pp 641–663, 1972.

[5] Gupta B and Loewy R. Theoretical analysis of the aerodynamic stability of multiple, interdigitated helical vortices. *AIAA J.*, Vol. 12, No. 10, pp 1381–1387, 1974.

[6] Ivanell S, Mikkelsen R, Sørensen J N and Henningson D S. Stability analysis of the tip vortices of a wind turbine. *Wind Energy*, Vol. 13, No. 8, pp 705–715, 2010.

[7] Sarmast S, Dadfar R, Mikkelsen R F, Schlatter P, Ivanell S, Sørensen J N and Henningson D S. Mutual inductance instability of the tip vortices behind a wind turbine. *Journal of Fluid Mechanics*, Vol. 755, pp 705–731, 2014.

[8] Quaranta H U, Brynjell-Rahkola M, Leweke T and Henningson D S. Local and global pairing instabilities of two interlaced helical vortices. *Journal of Fluid Mechanics*, Vol. 863, pp 927–955, 2019.

[9] Brocklehurst A and Barakos G N. A review of helicopter rotor blade tip shapes. *Progress in aerospace sciences*, Vol. 56, pp 35–74, 2013.

[10] Huang X, Moghadam S A, Meysonnat P, Meinke M and Schröder W. Numerical analysis of the effect of flaps on the tip vortex of a wind turbine blade. *Int. J. Heat Fluid Flow*, Vol. 77, pp 336–351, 2019.

[11] Marten D, Paschereit C O, Huang X, Meinke M, Schroeder W, Mueller J and Oberleithner K. Predicting wind turbine wake breakdown using a free vortex wake code. *AIAA Journal*, Vol. 58, No. 11, pp 4672–4685, 2020.

[12] Schröder D, Leweke T, Hörnschemeyer R and Stumpf E. Experiments on helical vortex pairs in the wake of a rotor. *AIAA Scitech 2021 Forum*, p. 1088. 2021.

[13] Venegas E D and Le Dizès S. Generalized helical vortex pairs. *J. Fluid Mech.*, Vol. 865, pp 523–545, 2019.

[14] Walther J H *et al.* A numerical study of the stability of helical vortices using vortex methods. *J. Phys. Conf. Ser.*, Vol. 75, p. 012034. IOP Publishing, 2007.

[15] Castillo-Castellanos A and Le Dizès S. Closely spaced co-rotating helical vortices: Long-wave instability. *arXiv preprint arXiv:2112.09211*, 2021.

[16] Castillo-Castellanos A, Le Dizès S and Venegas E D. Closely spaced corotating helical vortices: General solutions. *Physical Review Fluids*, Vol. 6, No. 11, p. 114701, 2021.

[17] Rosenhead L. The spread of vorticity in the wake behind a cylinder. *Proceedings of the Royal Society of London. Series A, Containing papers of a mathematical and physical character*, Vol. 127, No. 806, pp 590–612, 1930.

[18] Moore D W. Finite amplitude waves on aircraft trailing vortices. *The Aeronautical Quarterly*, Vol. 23, No. 4, pp 307–314, 1972.

[19] Saffman P G. *Vortex dynamics*. Cambridge university press, 1992.

[20] Leishman G J. *Principles of helicopter aerodynamics*. 2nd edition, Cambridge university press, 2006.

[21] Okulov V L and Sørensen J N. The self-induced motion of a helical vortex. *Journal of Fluid Mechanics*, Vol. 883, 2020.

[22] Martins J R R A, Sturdza P and Alonso J J. The complex-step derivative approximation. *ACM Trans. Math. Softw.*, Vol. 29, No. 3, pp 245–262, 2003.

[23] Bagheri S, Åkervik E, Brandt L and Henningson D S. Matrix-free methods for the stability and control of boundary layers. *AIAA J.*, Vol. 47, No. 5, pp 1057–1068, 2009.

[24] Gupta B P and Loewy R G. *Analytical Investigation of the Aerodynamic Stability of Helical Vortices Shed From a Hovering Rotor*. Tech. Rep. USAAMRDL TR-73-84, University of Rochester, 1973.

[25] Lamb H. *Hydrodynamics*. Cambridge University Press, 1932.

[26] Kleusberg E, Benard S and Henningson D S. Tip-vortex breakdown of wind turbines subject to shear. *Wind Energy*, Vol. 22, No. 12, pp 1789–1799, 2019.

[27] Kleine V G, Franceschini L, Carmo B S, Hanifi A and Henningson D S. The stability of wakes of floating wind turbines. *arXiv preprint arXiv:2203.11803*, 2022.

[28] Okulov V L and Sørensen J N. Stability of helical tip vortices in a rotor far wake. *J. Fluid Mech.*, Vol. 576, pp 1–25, 2007.

[29] Kleine V G, Kleusberg E, Hanifi A and Henningson D S. Tip-vortex instabilities of two in-line wind turbines. *Journal of Physics: Conference Series*, Vol. 1256, p. 012015. IOP Publishing, 2019.